

Analysis of ultraviolet photo-response of ZnO nanostructures prepared by electrodeposition and atomic layer deposition

Houssin Makhlouf, Chantal Karam, Amina Lamouchi, Sophie Tingry, Philippe Miele, Roland Habchi, Radhouane Chtourou, Mikhael Bechelany

▶ **To cite this version:**

Houssin Makhlouf, Chantal Karam, Amina Lamouchi, Sophie Tingry, Philippe Miele, et al.. Analysis of ultraviolet photo-response of ZnO nanostructures prepared by electrodeposition and atomic layer deposition. Applied Surface Science, 2018, 444, pp.253 - 259. 10.1016/j.apsusc.2018.02.289 . hal-01774661

HAL Id: hal-01774661

https://hal.umontpellier.fr/hal-01774661

Submitted on 4 Jun 2021

HAL is a multi-disciplinary open access archive for the deposit and dissemination of scientific research documents, whether they are published or not. The documents may come from teaching and research institutions in France or abroad, or from public or private research centers.

L'archive ouverte pluridisciplinaire **HAL**, est destinée au dépôt et à la diffusion de documents scientifiques de niveau recherche, publiés ou non, émanant des établissements d'enseignement et de recherche français ou étrangers, des laboratoires publics ou privés.

Analysis of Ultraviolet photo-response of ZnO nanostructures prepared by electrodeposition and atomic layer deposition

Houssin Makhlouf[1,2,3£], Chantal Karam[1,4£], Amina Lamouchi[2,3], Sophie Tingry[1], Philippe Miele[1], Roland Habchi[4], Radhouane Chtourou[2] and Mikhael Bechelany[1]

[1]Institut Européen des Membranes, IEM, UMR 5635, Université Montpellier, ENSCM, CNRS, Place Eugène Bataillon, F-34095 Montpellier Cedex5, France.

[2]Laboratoire de Nanomatériaux et Systèmes des Energies Renouvelables (LANSER), Centre de Recherches et des Technologies de l'Energie, Technopole BorjCedria, Bp 95, Hammam-Lif, 2050 Tunis, Tunisia.

[3]Faculté des sciences de Tunis, Université de Tunis, El Manar, 2092 Tunis, Tunisia.

[4]EC2M, faculty of sciences 2, Campus Pierre Gemayel, Lebanese University,90656, Lebanon.

[£]These authors contributed equally to the paper.

ABSTRACT

In this work, ZnO nanowires (ZnO NWs) and urchin-like ZnO nanowires (U-ZnO NWs) based on self-assembled ordered polystyrene sphere (PS) were successfully prepared by combining atomic layer deposition (ALD) and electrochemical deposition (ECD) processes to build UV photosensors. The photo-response of the prepared samples was investigated and compared. The growth of the nanowires on self-assembled ordered PS introduce a significant modification on the morphology, crystal orientation and grain size of U-ZnO NWs compared to randomly vertically aligned ZnO NWs and therefore improve the photo-response of U-

ZnONWs. The photocurrent might be produced by either surface or bulk-related process. For ZnO NW-based photosensor, the photocurrent was monitored by a surface related process, whereas, it was mainly governed by a bulk related process for U-ZnO NWs, resulting in a higher and faster photo-response. The study of the rise and decay time constants for both materials showed that these parameters were strikingly sensitive to the optical properties.

KEYWORDS: urchin-like ZnO nanowires, electrochemical deposition, atomic layer deposition, photoconductivity, UV sensor.

INTRODUCTION

Thanks to their great potential, zinc oxide (ZnO) nanostructures have been studied for diverse applications including solar cells,[1] photocatalysts,[2] and sensors.[3-4] The performance of the ZnO nanostructures devices like nanowires and nanobelts was improved owing to the several properties of these nanostructures, such as wide band gap of 3.37 eV, wide exciton bending energy (60 meV) and high electron mobility (120 cm^2 V^{-1} S^{-1}).[5] Recently, the researchers have focused on using ZnO nanowires as ultraviolet (UV) photo-response sensor thanks to their fast response,[6] high photocurrent[7] and high sensitivity to UV light[8-9] as a result of the surface to volume ratio improvement of the nanowires compared to ZnO films.[10]

The photoconductivity phenomenon in ZnO is generally related to adsorption and desorption of the chemisorbed oxygen from the surface of ZnO.[11] A high-performance photodetector is characterized by an excellent response/recovery time, and fast raise time constants[12]. In the literature, several parameters have been investigated that give rise to a higher UV photo-response behavior. Bera and Basak showed enhancement of the UV photo-response of ZnO when the nanowires were capped with poly(vinyl alcohol) (PVA).[13] Similarly, Lao *et al.* detected an enhanced UV photo-response based on ZnO nanobelts which was attributed to the

surface functionalization with different polymers.[9] On the other hand, Tzenga *et al*. reported an enhancement in the performance of Ag/ZnO NWs heterostructure by adding Silver nanoparticles to the nanowires. This enhancement was assigned to the formation of Shottky barriers at the interface of Ag and ZnO NWs.[14] According to Suobai *et al*., the photo-response increased when multiple ZnO NWs are connected in parallel via the contact printing method.[15] UV light irradiance is also a crucial parameter which determines the sensitivity of ZnO to UV light. In this context, Yanbo *et al.* postulated that ZnO bridging nanowires grown by chemical vapor deposition could detect irradiance down to 10^{-8} w/cm^2. [16] Other physicho-chemical parameters such as crystallographic orientation, grain size,[17] annealing treatment[18] and high defects concentration[19] have contributed to the enhancement of the photo-response of ZnO NWs device.

So far, various techniques have been used to synthesize ZnO UV sensors such as nanoparticle-assisted pulsed-laser deposition (NAPLD),[20] chemical vapor deposition (CVD),[21] metalorganic chemical vapor deposition (MOCVD),[22] hydrothermal method,[23] pulsed laser deposition(PLD),[24] atomic layer deposition (ALD) and electrochemical deposition (ECD).[25] Among these techniques, the ALD technique results in the preparation of conformal films with sub-nanometer thickness control,[26-27] while ECD offers a considerable scale production of aligned ZnO nanowires on various substrates.[1]

In the present work, we report the combination of the two scalable ALD and ECD techniques for preparing ZnO NWs and U-ZnO NWs based photodetectors. Structural, optical and photo-response properties of the obtained materials were investigated to show how the morphology, the crystal orientation and the grain size influence the photocurrent behavior under UV light illumination and affect the performance of the UV photodetectors (fast rise and decay time constants).

MATERIALS AND METHODS

1. Materials

Zinc chloride ($ZnCl_2$), potassium chloride (KCl) and diethyl zinc (DEZ) ($Zn(CH_2CH_3)_2$, 95%) were purchased from Sigma Aldrich and used as received. The ITO coated glass substrates were purchased from KINTEC Company, Hong Kong.

A commercially available polystyrene microsphere (PS) suspension (diameter ~5 µm, 4 wt % aqueous dispersion) from Thermo fisher, USA, was used to dip coat of a transparent indium-doped tin oxide (ITO) glass (size (1x5) cm^2) purchased from Kintec Company, Hong Kong. The initial substrates consisted of a ~120 nm thick ITO layer (resistivity 10 Ω.m) on glass. The ITO substrates were cleaned using successively acetone and isopropanol in an ultrasonic bath (15 min each) and then rinsed with water before depositing the PS spheres and the ZnO seed layer.

2. Synthesis of ZnO NWs and ZnO Urchins (U-ZnO NWs)

a) Atomic layer deposition of ZnO seed layer.

ZnO seed layers were deposited by ALD process on ITO substrate prior to the growth of ZnO NWs by ECD. ALD of ZnO was carried out in a home-built reactor using sequential exposures of DEZ and H_2O separated by argon purge at a chamber temperature of 80°C (at flow rates of 100 sccm). Briefly, the process consisted of 0.2 s pulse and 40 s exposure of DEZ, 60 s of argon purge followed by 2 s pulse and 40 s exposure of H_2O, and a final 60 s argon purge to complete the ALD cycle.[28] In order to prepare 20 nm thick ZnO seed layers, 100 ALD cycles were carried out.[29]

Two samples were prepared: one sample, named ZnO_{ALD}\ITO, with a 20 nm ZnO thick seed layer directly deposited on ITO , and a second sample, named ZnO_{ALD}\PS\ITO, with a 20 nm ZnO thick seed layer deposited on self-assembled ordered polystyrene spheres (PS) organized

on ITO substrate according to a procedure described in our previous work.[30] The ZnO seed layer on the PS was employed to control the growth of the nanowires in order to synthesize the 3D urchin-like ZnO NWs structures.

b) Electrochemical deposition of nanowires

The ECD process was performed in a classical three-electrode electrochemical cell for the electrodeposition of nanowires. The ZnO_{ALD}\ITO and ZnO_{ALD}\PS\ITO were used as working electrodes and were immersed in an aqueous solution containing 5.10^{-4} M $ZnCl_2$ and 0.1 M KCl (under continuous bubbling of oxygen).[31-32] The electrodeposition was carried out at the fixed potential of -1.0 V versus Ag/AgCl using an Autolab PGSTAT30 potentiostat. The deposition time was 240 minutes and the reaction temperature was kept at 80°C.[33-34] The obtained samples were named ZnO NWs and U-ZnO NWs resulting from the modification of ZnO_{ALD}\ITO and ZnO_{ALD}\PS\ITO, respectively.[35]

3. Chemical and structural characterizations

Morphological properties were investigated by Scanning electron microscopy (SEM) using a HITACHI-S4800 and energy dispersive X-Ray spectroscopy using a HITACHI S-4500, coupled with a Thermofisher EDX detector. The crystallinity studies have been carried out using powder XRD with a PANalyticalXpert-PRO diffractometer (Cu Kα radiation). The transmission measurements were performed using a UV/Vis/NIR spectrophotometer (Jasco V-570). Photoluminescence measurements were achieved at room temperature using HORIBA JobinYvon spectrometer with 266 nm excitation wavelength laser.

4. UV sensor measurement

In order to study the photo-detection properties of the samples, electrical measurements were performed both under dark and UV illumination.

A UV-lamp (365 nm) was used for UV illumination. The radiation power of the 365 nm UV source illuminating the sample device was 1.87 mW/cm^2. The humidity was about 41%.

Top contacts were made using two lines silver deposited manually on the sample's surface with a separation of 5 mm in order to facilitate the handling and to perform the electrical measurements, as depicted in Figure 1.

Sweep voltammetry and chronoamperometry measurements were performed using a potentiostat (EG&G instruments, 265 A model). Sweep voltammetry was carried out from -3 V to 3 V with a scanning speed of 50 mV/s. Chronoamperometry measurements were performed with on/off UV illumination at -1 V during 3000 s using the following protocol[36]: UV off between 0 and 100 s, UV on between 100 and 200 s, finally UV off between 200 and 3000 s. The UV photo-response data was extracted from chronoamperometry experiments. The photo-response current ΔI was defined as the difference between current under UV illumination and current under dark.

RESULTS AND DISCUSSION

1. Morphology and microstructure

The examination of the ZnO NWs and U-ZnO NWs by SEM, Figure 2, shows that the NWs prepared by electrodeposition are uniformly distributed and grown along a preferred quasi-vertical direction on the ZnO thick seed layers (Figure 2a and 2b). The average diameter and length of the nanowires are ~ 950 nm and ~ 80 nm respectively (Figure 2c). The morphology of the nanowires changes when they are electrodeposited

on the PS covered with ZnO ALD seed layers. Once the electrodeposition of ZnO NWs has been carried out, the nanowire grew homogeneously on the ALD ZnO layers covering the entire surface of PS and forming a 3D organization of U-ZnO NWs building-blocks (Figure 2d, 2e and 2f), the size of the spheres is around 4 µm, while the average diameter and length of the nanowires are ~ 950 nm and ~ 50 nm, respectively.

The microstructure of the samples was investigated by XRD analysis, as shown in Figure 3. The presence of hexagonal ZnO is revealed by the peaks observed at 31.6° ; 34.3° ; 36.3° and 47.5° , corresponding respectively to the (100), (002), (101), and (102) planes. For the ZnO NWs sample, the intensity of the (002) peak is stronger than the others, suggesting that the nanowires are highly oriented with the *c*-axis. However, for the U-ZnO NWs, the same XRD peaks are observed but with lower intensities. Due to the 3D organization of the nanowires in the urchin sample, they grew less textured than the ZnO NWs arrays. This 3D organization involves a [(100), (002), (101), and (102)] mixed crystallographic orientation for the U-ZnO NWs sample. The average grain size of the prepared samples was calculated using the Debye-Scherrer relation. The calculated value was 35.41 nm for ZnO NWs and 16.52 nm for U-ZnO NWs.

2. Optical analysis

Figure 4 (A) shows the optical transmission spectra of ZnO NWs and U-ZnO NWs. The transmittance in the visible region is less than 30%. This low transparency into the visible range can be attributed to the imperfect vertical alignment of the nanowires. As seen in the SEM images (Figure 2), for both samples, many nanowires were inclined along the ZnO thick seed layers. This arrangement of the nanowires caused aimless scattering of the incident light between the nanowires (voids). Thus, the scattering reduced the optical transmittance into the

visible range. The optical band gap Eg for the two materials was calculated using the Tauc formula.[33] We estimated the optical band gap energy of U-ZnO NWs and ZnO NWs to be 3.22 eV and 3.13 eV respectively (Figure S1). Compared to the typical band gap of ZnO around 3.3-3.4 eV,[5] one can deduce that the two prepared samples present intermediate energy levels in the band gap of ZnO. The variation of $(\alpha h\upsilon)^2$ versus $h\upsilon$ curves of the samples is far away from the zero band edge confirming also the presence of several intermediate energy levels within the band gap. These intermediate energy levels act as a trap or/and recombination center for the photogenerated carriers[37]. PL measurements were performed to investigate the optical properties of the prepared samples. Figure 5 shows the room temperature PL spectra of ZnO NWs and U-ZnO NWs. These two spectra exhibit a strong UV emission peak around 382 nm and a weak broad emission in the visible range into 450-650 nm. In addition, the intensity of the UV emission peak for U-ZnO NWs is higher than that of the ZnO NWs.

The UV emission peak can be attributed to the near-band-edge (NBE) in the ZnO[21, 38] while the visible band emission is assigned to electronic states into the band gap which are related to the intrinsic defect of ZnO[39]. The decay of the NBE intensity of ZnO NWs involves the high intrinsic defects density within the gap which acts as a trap or recombination center for the photogenerated electron\holes pairs.

3. UV sensing measurements

Figure 6 shows the I-V characteristic of ZnO NWs and U-ZnO NWs. The curves indicate a good connection between the ZnO nanowires and the Ag contact confirming the ohmic contact of the Ag/ZnO NWs. The values of I_{Dark}, I_{UV} and I_{Dark}/I_{UV} ratios are listed in table 1.

We can clearly observe that ZnO NWs deliver higher current in the dark than under illumination, while U-ZnO NWs exhibit an opposite behavior that results finally in a slight

difference of the I_{Dark}/I_{UV} ratio from 1.28 for ZnO NWs to 1.11 for U-ZnO NWs. These ratios close to the unity indicate the presence of a wide amount of intrinsic donor defects which are assigned to ZnO n-type.

The UV photo-response current (ΔI) was obtained by chronoamperometry measurement under the UV light illumination intensity of 1.87 mW/cm^2 (Figure7). The UV photo-response of the ZnO sensors (A/W) was determined from the ratio between the electrical output ΔI and the optical input (UV source's power). These parameters are summarized in table 1. We note here that additional tests (not shown here) were performed and proved that the obtained results are reproducible.

As observed in Figure 6, in the presence of the NWs, the photo-response of ZnO increases gradually with time under UV illumination reaching an intensity of 0.026 A. When the UV light is switched off, the photo-response decays slowly and the initial value is re-established. For the U-ZnO NWs material, the photo-response increases first rapidly and then rises relatively slow under UV light illumination reaching a maximum intensity of 0.048A. When UV is switched off, the photo-response decay is sharp during a few seconds without reaching the initial state.

The difference of the photo-response between the urchins and the NWs is related to the oxygen adsorption/desorption onto the ZnO that occurs by a process involving either the surface or the bulk of the material[11]. From the EDX results presented in the supporting information (Table S1), the O/Zn ratio is greater than unity for both samples, meaning that an excess of oxygen is trapped on the grain boundaries of ZnO. In addition, the two following observations: (i) the small grain size of U-ZnO NWs (16.52 nm) compared to ZnO NWs (35.41 nm) attributed to more grain boundaries developed in U-ZnO NWs, and (ii) the smaller dark current founded for ZnO NWs attributed to higher numbers of trapped carriers because of the poor amount of

adsorbed O_2,[13] suggest that U-ZnO NWs photo-response is mainly governed by the bulk-related process, whereas for ZnO NWs the photo-response current is monitored by the surface related process.

When materials are characterized by adsorption/desorption of oxygen at ZnO NWs surface, in the dark, the oxygen molecules take free electrons to form a barrier near the surface of the nanowires. Then under UV light illumination, the photo-generation of electron-hole pairs occurs and consequently, the holes discharge the oxygen ions chemisorbed on the surface and eliminate the barrier. Electrons produced at the same time increase the conductivity of the ZnO nanowires.[18]

However, when adsorption/desorption of oxygen rather occurs in the bulk of materials, the photo-response is consistent with the changes of the barrier heights on grain boundaries trapped in the bulk. Under UV light, an excess of oxygen photo-desorbed on grain boundaries decreases the barrier heights of grain boundaries,[11] thus the photo-response of the U-ZnO NWs increases. Under dark, the oxygen photo-desorbed from grain boundaries will be chemisorbed again leading to the decrease of the photo-response of U-ZnO NWs.

It was reported that bulk related process gives higher and faster photo-response in comparison to surface related process.[40] Another photoconductivity mechanism related to the different morphology of the two photosensors devices may explain the photo-response improvement of the U-ZnO NWs. In fact, the growth of the nanowires on PS induces a significant physical contact of U-ZnO NWs compared to randomly vertically aligned ZnO NWs as seen in the SEM images (Figure 2c and 2f). This physical contact results in junction barrier between two neighbor urchins. Upon UV illumination, the junction barrier decreases [41] and the electrons have to overcome the U-ZnO NW - U-ZnO NW barrier when tunneling from one U-ZnO NW to another leading to the increase of photocurrent.

In the present study, the fast rise in the photo-response of U-ZnO NWs (detected in the first 3 second after the UV light was on, Figure 7) can be attributed to the bulk related process. However, the presence of trap levels in the samples results in a slower rise of the photo-response at longer times, similar to that observed for ZnO NWs.

It is worth noting that if the trap levels are absent, the photo-response rises quickly. In order to evaluate the rise time constants, the photocurrent rise can be fitted with single exponential rise equation:

$$I = I_0(1-\exp(-t/\tau))$$

Where I_0 is the dark current and τ is the time constant for rising photocurrent. The fitted curves are shown in Figure S2 (a). The rise time constant was found to be 28.49 s and 83.33 s for U-ZnO NWs and ZnO NWs, respectively. The traps center present in U-ZnO NWs (shallow/deep levels with respect to the valence/conduction band) can captivate the photo-generated charge carriers and increase their lifetime before they jump to the conduction band. On the other hand, the chemisorption of oxygen species on the NWs surface is considered as a slow process[16] where the oxygen species may act as shallow traps.[11] This effect leads to an extended rise time constant of 83.33s for ZnO NWs comparing to 28.49s obtained for U-ZnO NWs. Therefore, it highlights the important role of U-ZnO NWs which becomes significant during the first seconds on the photo-response current, where the bulk related process dominates and results in higher and fast photo-response. Once the UV light is off, the photocurrent decay can be fitted with second-order exponential decay equation:

$$I = A_1(\exp(-t/\tau_1)) + A_2(\exp(-t/\tau_2)) + I_0 \text{ ; for U-ZnO NWs}$$

$$I = A_3(\exp(-t/\tau_3)) + A_4(\exp(-t/\tau_4)) + I_0 \text{ ; for ZnO NWs}$$

where A_1, A_2, A_3 and A_4 are positive constants, I_0 is dark current, and τ_1, τ_2, τ_3 and τ_4 are the time constants for decaying photocurrent. The resulting curves are shown in Figure S2 (b). The calculated decay time constants for the two samples are equal to $\tau_1 =$ 60.29 s, $\tau_2 =$ 700.47 s for U-ZnO NWs and $\tau_3 =$ 120.05 s, $\tau_4 =$ 1372 s for ZnO NWs. These values indicate the presence of two different decay mechanisms: fast (τ_1, τ_3) and slow (τ_2, τ_4) relaxation time constants. In addition, one can note that the carrier relaxation in U-ZnO NWs is faster than that in ZnO NWs.

Conventionally, the photo-response decay is governed by the i) re-adsorption of oxygen and ii) recombination of electron-hole and electron recombination centers.

The re-adsorption is known as a slow process.[42] Hence, the fast decay time τ_1 is related to the bulk process and the slow decay time τ_2 can be assigned to there-adsorption of oxygen species.

Usually, the recombination of electron-hole pairs takes place with fast decay times if the recombination occurs band to band.[43] However, the relaxation time increases when the sample presents recombination centers which extend the decay time.[44] In our study, the slow decay times (τ_3, τ_4) are attributed to the electron recombination centers. τ_4 is longer than τ_3 due to the excessive recombination centers present on the ZnO NWs compared to the U-ZnO NWs. Therefore, the trap/recombination centers are responsible for the observed faster and decay photocurrent growth for U-ZnO NWs. This finding is in a good agreement with optical results.

CONCLUSION

ZnO nanostructures were successfully prepared by combining ALD and ECD techniques to build UV photosensors. A considerable improvement in the photo-response

was detected for the photosensors based on U-ZnO NWs compared to ZnO NWs. The changes observed in the morphology, crystal orientation and grain size between the two materials induced a variation in the photoconductivity phenomenon which indicates the presence of two processes whose origin is surface and bulk-related process for ZnO NWs and U-ZnO NWs, respectively. The photocurrent rise\decay was fitted with an exponential rise\decay equation. The U-ZnO NWs exhibited faster rise and smaller decay time constant in comparison with the ZnO NWs. These deductions were proved by optical measurements. This novel technique is a very promising method since it offers a synthesis of ZnO nanostructures suitable for a UV sensors application.

REFERENCES:

[1] J.W. Chen, D.C. Perng, J.F. Fang, Nano-structured Cu_2O solar cells fabricated on sparse ZnO nanorods, Solar Energy Materials and Solar Cells. 95 (2011) 2471–2477.

[2] S. Moradi, P.A. Azar, S.R. Farshid, S.A. Khorrami, M.H. Givianrad, Effect of Additives on Characterization and Photocatalytic Activity of Tio_2/ZnO Nanocomposite Prepared via Sol-Gel Process, International Journal of Chemical Engineering. 215373 (2012) 1–5.

[3] M. Drobek, J-H. Kim, M. Bechelany, C.Vallicari, A. Julbe, S.S. Kim, MOF-Based Membrane Encapsulated ZnO Nanowires for Enhanced Gas Sensor Selectivity, Appl. Mater. Interfaces. 8 (2016) 8323–8328.

[4] M.H. Mamat, Z. Khusaimi, M.Z. Musa, M.F. Malek, M. Rusop, Physical Fabrication of ultraviolet photoconductive sensor using a novel aluminium-doped zinc oxide nanorod – nanoflake network thin film prepared via ultrasonic-assisted sol–gel and immersion methods, Sensors and Actuators: A. Physical. 171 (2011) 241–247.

[5] M. Abd-Ellah, J.P. Thomas, L. Zhang, K.T. Leung, Enhancement of solar cell performance of p-Cu_2O/n-ZnO-nanotube and nanorod heterojunction devices, Solar Energy Materials and Solar Cells. 152 (2016) 87–93.

[6] J. Sun, F-J. Liu, H-Q. Huang, J-W. Zhao, Z-F. Hu, X-Q. Zhang, Y-S. Wang, Fast response ultraviolet photoconductive detectors based on Ga-doped ZnO films grown by radio-frequency magnetron sputtering, Applied Surface Science. 257 (2010) 921–924.

[7] J.P. Kar, S.N. Das, J.H. Choi, Y.A. Lee, T.Y. Lee, J.M. Myoung, Fabrication of UV detectors based on ZnO nanowires using silicon microchannel, Journal of Crystal Growth. 311 (2009) 3305–3309.

[8] H. Jeong, K.S. Kim, Y.H. Kim, H. Jeong, H. Song, K.H. Lee, M.S. Jeong, D. Wong, J.Y. Jung, A crossbar-type high sensitivity ultraviolet photodetector array based on a one hole–one nanorod configuration via nanoimprint lithography, Nanotechnology. 22 (2011) 8.

[9] C.S. Lao, M-C. Park, Q. Kuang, Y. Deng, A.K. Sood, D.L. Polla, Z.L. Wang, Giant Enhancement in UV Response of ZnO Nanobelts by Polymer Surface-Functionalization, Journal of the American Chemical Society. 129 (2007) 12096–12097.

[10] A. Abou Chaaya, M. Bechelany, S. Balme, P. Miele, ZnO 1D nanostructures designed by combining atomic layer deposition and electrospinning for UV sensor applications, Journal of Materials Chemistry A. 2 (2014) 20650–20658.

[11] S.Kumar, G-H. Kim, K Sreenivas, R.P. Tandon, Mechanism of ultraviolet photoconductivity in zinc oxide nanoneedles, Journal of Physics-Condensed Matter. 19 (2010) 1–10.

[12] D. Gedamu, I. Paulowicz, S. Kaps , O. Lupan, S. Wille, G. Haidarschin , Y.K. Mishra, R. Adelung, Rapid Fabrication Technique for Interpenetrated ZnO Nanotetrapod Networks for Fast UV Sensors, Advanced Materials. 26 (2014) 1541–1550 (2014).

[13] A. Bera, D. Basak, Effect of Surface Capping with Poly(vinyl alcohol) on the Photocarrier Relaxation of ZnO Nanowires, Acs Applied Materials & Interfaces. 1 (2009) 2066–2070.
[14] S. Tzeng, M. Hon, I. Leu, Improving the Performance of a Zinc Oxide Nanowire Ultraviolet Photodetector by Adding Silver Nanoparticles, Journal of the Electrochemical Society. 159 (2012) H440–H443.
[15] S. Bai, W. Wu, Y. Qin, N. Cui, D.J. Bayerl, X. Wang, High - Performance Integrated ZnO Nanowire UV Sensors on Rigid and Flexible Substrates, Advanced Functional Materials. 21 (2011) 4464–4469.
[16] Y. Li, F. Della Valle, M. Simonnet, I. Yamada, J-J. Delaunay, High-Performance UV Detector made of ultra-long ZnO bridging nanowires, Nanotechnology. 20 (2009) 1–5.
[17] J.B.K. Law, J.T.L. Thong, Simple fabrication of a ZnO nanowire photodetector with a fast photoresponse time, Appl. Phys. Lett. 88 (2006) 13–15.
[18] M.H. Mamat, M. Izzudin, C. Khalin, N. Noor, H. Nik, Z. Khusaimi, N.D. Sin, S.S. Shariffudin, M.M. Zahidi, M.R. Mahmood, Effects of Annealing Environments on the Solution-Grown , Aligned Aluminium-Doped Zinc Oxide Nanorod-Array-Based Ultraviolet Photoconductive Sensor, Journal of Nanomaterials. 189279 (2012) 1–15.
[19] A. Physics, T. Indore, A. Faisalabad, S. Age, N. Rates, R. View, A.K. Kushwaha, Defect induced high photocurrent in solution grown vertically aligned ZnO nanowire array films, J. Appl. Phys. 112 (2012) 1–7.
[20] J. Suehiro, N. Nakagawa, S-i. Hidaka, M. Ueda, K. Imasaka, M. Higashihata, T. Okada, M. Hara, Dielectrophoretic fabrication and characterization of a ZnO nanowire-based UV photosensor, Nanotechnology. 17 (2006) 2567–2573 (2006).
[21] O. Lupan, G. Chai, L. Chow, G. A. Emelchenko, H. Heinrich, V. V. Ursaki, A. N. Gruzintsev, I. M. Tiginyanu, A. N. Redkin, Ultraviolet photoconductive sensor based on single ZnO nanowire, Phys. Status Solidi A. 207 (2010) 1735–1740.
[22] M. Rosina, P. Ferret, P. Jouneau, I. Robin, F. Levy, G. Feuillet, M. Lafossas, Morphology and growth mechanism of aligned ZnO nanorods grown by catalyst-free MOCVD, Microelectronics Journal. 40 (2009) 242–245.
[23] O. Lupan, L. Chow, G. Chai, L. Chernyak, O. Lopatiuk-tirpak, H. Heinrich, Focused-ion-beam fabrication of ZnO nanorod-based UV photodetector using the in-situ lift-out technique, Phys. Status Solidi A. 205 (2008) 2673–2678.
[24] G.M. Fuge, T.M.S. Holmes, M.N.R. Ashfold, Ultrathin aligned ZnO nanorod arrays grown by a novel diffusive pulsed laser deposition method, Chemical Physics Letters. 479 (2009) 125–127.
[25] G. She, C. Academy, Z. Liao, O. Ridge, Z. Liao, Observation of persistent photoconductance in single ZnO nanotube, Applied Physics Letters . 94 (2009) 1–3.
[26] I. Iatsunskyi, A. Vasylenko, R. Viter, M. Kempiński, G. Nowaczyk, S. Jurga, M. Bechelany, Tailoring of the electronic properties of ZnO-polyacrylonitrile nanofibers: Experiment and theory, Applied Surface Science. 411 (2017) 494–501.
[27] R. Viter, I. Iatsunskyi, V. Fedorenko, S. Tumenas, Z. Balevicius, A. Ramanavicius, S. Balme, M. Kempiński, G. Nowaczyk, S. Jurga, M. Bechelany, Enhancement of Electronic and Optical Properties of ZnO/Al_2O_3 Nanolaminate Coated Electrospun Nanofibers, Journal of Physical Chemistry C. 120 (2016) 5124–5132.
[28] S. Cabello-Aguilar, S. Balme, A. Abou Chaaya, M. Bechelany, E. Balanzat, J-M. Janot, C. Pochat-Bohatier, P. Mielea, P. Dejardina, Slow translocation of polynucleotides and their discrimination by α-hemolysin inside a single track-etched nanopore designed by atomic layer deposition. 5 (2013) 9582–9586.
[29] G M. Baitimirova, R. Viter, J. Andzane, A. van.der.Lee, D. Voiry, I. Iatsunskyi, L.E. Coy, L. Mikoliunaite, S. Tumenas, K. Załęski, Z. Balevicius, I. Baleviciute, A.

Ramanaviciene, A. Ramanavicius, S; Jurga, D. Erts, M. Bechelany, Tuning of Structural and Optical Properties of Graphene/ZnO Nanolaminates, J. Phys. Chem. C. 120 (2016) 23716–23725. doi:10.1021/acs.jpcc.6b07221.

[30] C. Karam, C. Guerra-nuñez, R. Habchi, Z. Herro N. Abboud, A. Khoury, S. Tingry, P. Miele, I. Utke, M. Bechelany, Urchin-inspired ZnO-TiO_2 core-shell as building blocks for dye sensitized solar cells, Materials & Design. 126 (2017) 314-321.

[31] S. Peulon, D. Lincot, Mechanistic Study of Cathodic Electrodeposition of Zinc Oxide and Zinc Hydroxychloride Films from Oxygenated Aqueous Zinc Chloride Solutions, Journal of The Electrochemical Society. 145 (1998) 864–874.

[32] R. Tena-zaera, A. Katty, S. Bastide, C.Lévy-Clément, B.O'Regan, V.Muñoz-Sanjosé, ZnO/CdTe/CuSCN, a promising heterostructure to act as inorganic eta-solar cell, Thin Solid Films 483 (2005) 372–377.

[33] H. Makhlouf, O. Messaoudi, A. Souissi, I. Ben Assaker, M. Oueslati, M. Bechelany, R. Chtourou, Tuning of Ag doped core−shell ZnO NWs/Cu_2O grown by electrochemical deposition, Materials Research Express. 2 (2015) 95002.

[34] H. Makhlouf, M. Weber, O. Messaoudi, S. Tingry, M. Moret, O. Briot, R. Chtoutou, M. Bechelany, Study of Cu_2O\ ZnO nanowires heterojunction designed by combining electrodeposition and atomic layer deposition, Applied Surface Science. 426 (2017) 301–306.

[35] J. Elias, I. Utke, S. Yoon, M. Bechelany, A. Weidenkaff, J. Michler, L. Philippe, Electrochemical growth of ZnO nanowires on atomic layer deposition coated polystyrene sphere templates, Electrochimica Acta. 110 (2013) 387–392.

[36] R. Alchaar, H. Makhlouf, N. Abboud, S. Tingry, R. Chtourou, M. Weber, M. Bechelany, Enhanced UV photosensing properties of ZnO nanowires prepared by electrodeposition and atomic layer deposition, Journal of Solid State Electrochemistry. 21 (2017) 2877–2886.

[37] P. Sharma, K. Sreenivas, K.V. Rao, Analysis of ultraviolet photoconductivity in ZnO films prepared by unbalanced magnetron sputtering, Journal of Applied Physics. 93 (2003) 3963–3970.

[38] O. Lupan, T. Pauporté, B. Viana, Low-voltage UV-electroluminescence from ZnO-Nanowire array/p-CaN light-emitting diodes, Advanced Materials. 22 (2010) 3298–3302.

[39] R. Mimouni, A. Souissi, A. Madouri, K. Boubaker, M. Amlouk, High photocatalytic efficiency and stability of chromium-indium codoped ZnO thin films under sunlight irradiation for water purification development purposes, Current Applied Physics. 17 (2017) 1058–1065.

[40] D.H. Zhang, Fast photoresponse and the related change of crystallite barriers for ZnO films deposited by RF sputtering, Journal of Physics D-Applied Physics, 28 (1995) 1273–1277.

[41] M. Chen, L. Hu, J. Xu, M. Liao, L. Wu, X. Fang, ZnO Hollow-Sphere Nanofilm-Based High-Performance and Low-Cost Photodetector, small. 7 (2011) 2449–2453.

[42] S. Dhara, P.K. Giri, Enhanced UV photosensitivity from rapid thermal annealed vertically aligned ZnO nanowires, Nanoscale Research Letters. 6 (2011) 1–8.

[43] Y. Lang, H. Gao, W. Jiang, L. Xu, H. Hou, Photoresponse and decay mechanism of an individual ZnO nanowire UV sensor, Sensors and Actuators A : Physical. 174 (2012) 43–46.

[44] A. Bera and D. Basak, Role of defects in the anomalous photoconductivity in ZnO nanowires, Applied Physics Letters. 112 (2012) 1–7.

Figure 1. Schematic of the device with silver contacts.

Figure 2. SEM images of: (a-b-c) ZnO Nws and (d-e-f) U-ZnO NWs, with different magnifications.

Figure 3. XRD patterns of ZnO NWs and U-ZnO NWs.

Figure 4. Transmission spectra of: (A) ZnO NWs and U-ZnO NWs and (B) magnification of the spectra in the region of 360-415 nm.

Figure 5. Room Temperature PL spectra of ZnO NWs and U-ZnO NWs.

Figure 6. I-V curves of: (A) ZnO NWs and (B) U-ZnO NWs under dark (black curves) and UV illumination (red curves).

Figure 7. Intensity versus time curves under UV illumination at 365 nm for ZnO NWs and U-ZnO NWs materials.

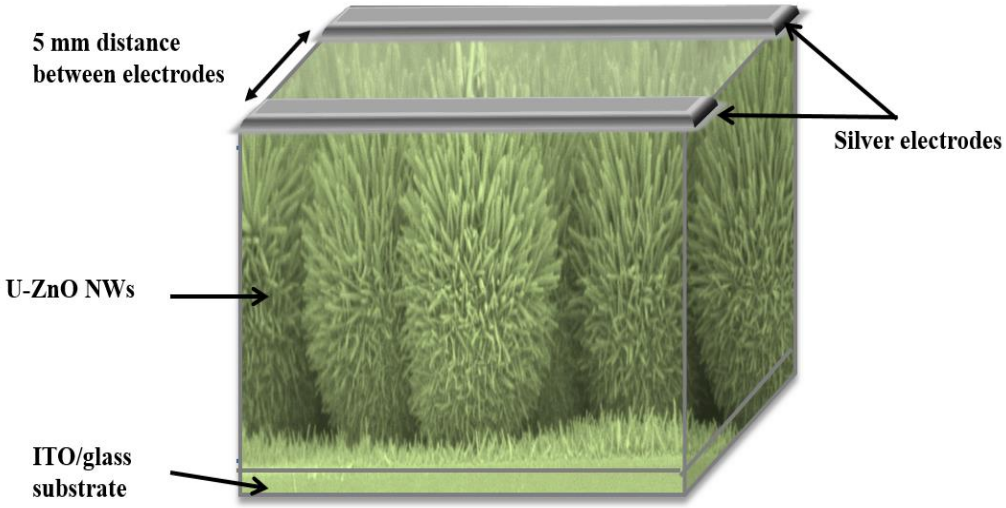


Figure 1. Schematic of the device with silver contacts.

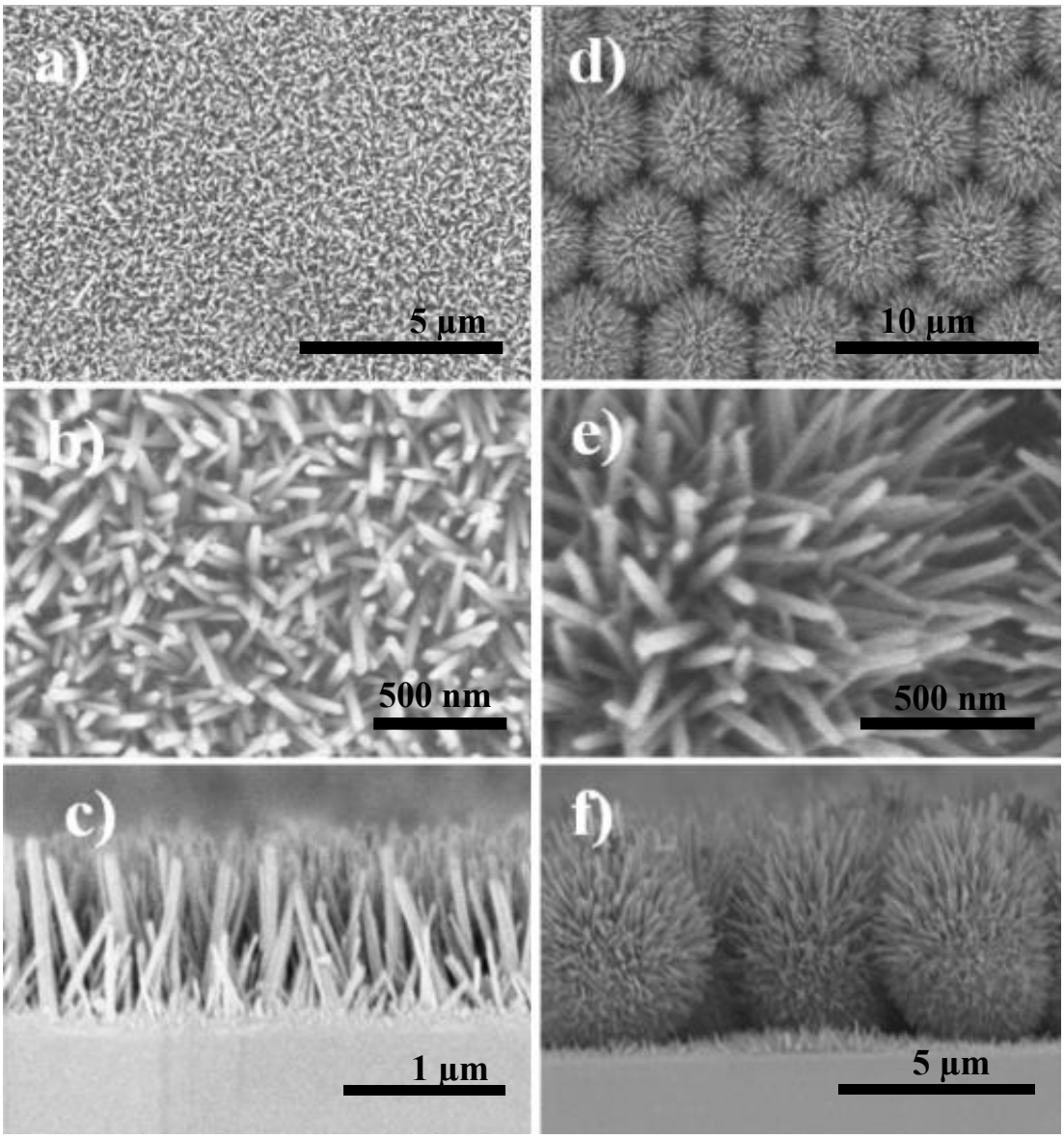


Figure 2. SEM images of: (a-b-c) ZnO NWs and (d-e-f) U-ZnO NWs, with different magnifications.

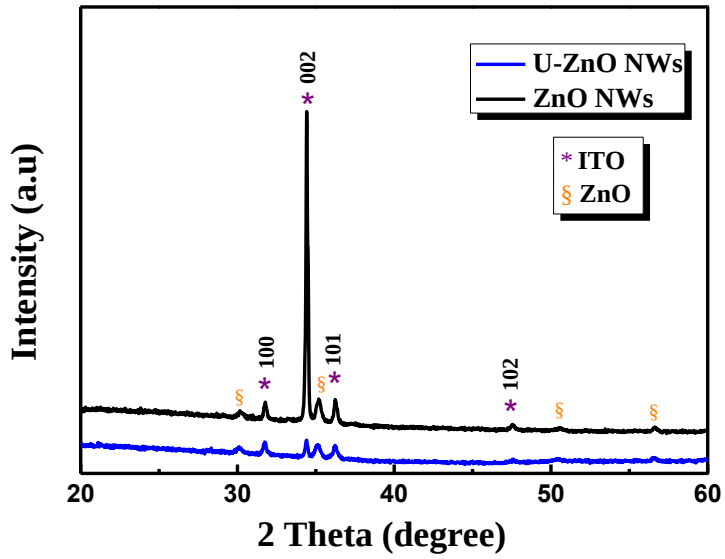


Figure 3. XRD patterns of ZnO NWs and U-ZnO NWs.

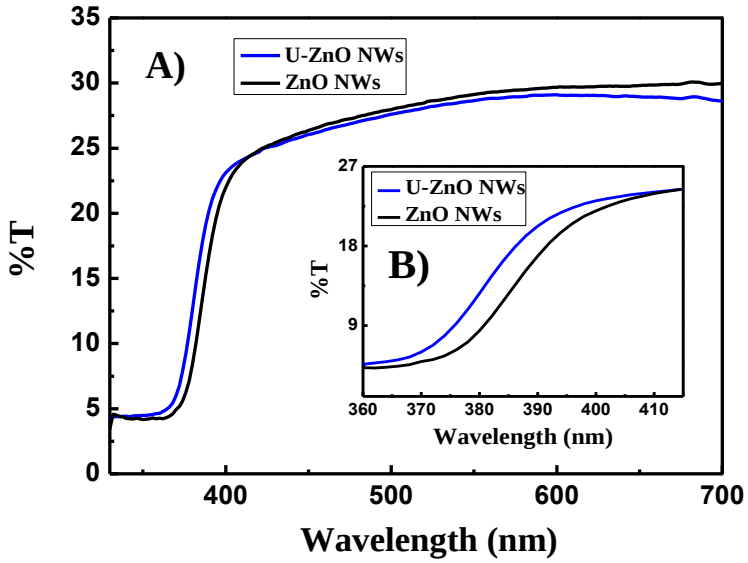


Figure 4. Transmission spectra of: (A) ZnO NWs and U-ZnO NWs and (B) magnification of the spectra in the region of 360-415 nm.

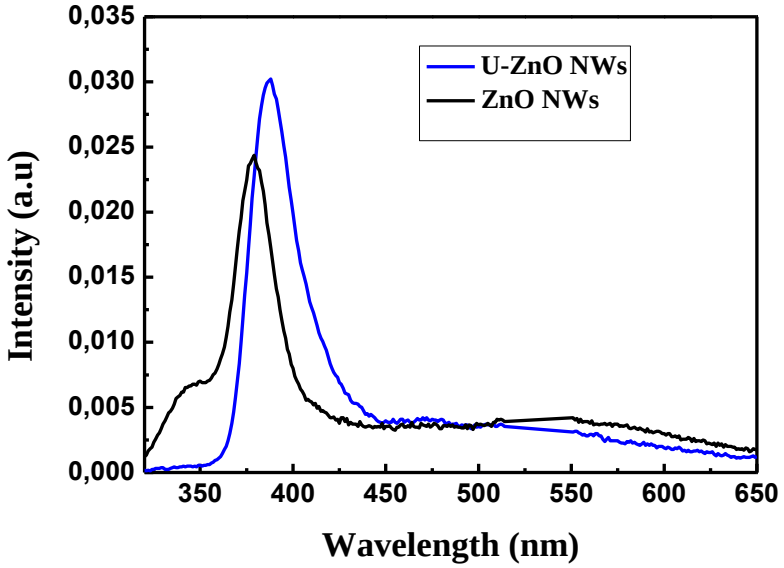


Figure 5. Room Temperature PL spectra of ZnO NWs and U-ZnO NWs.

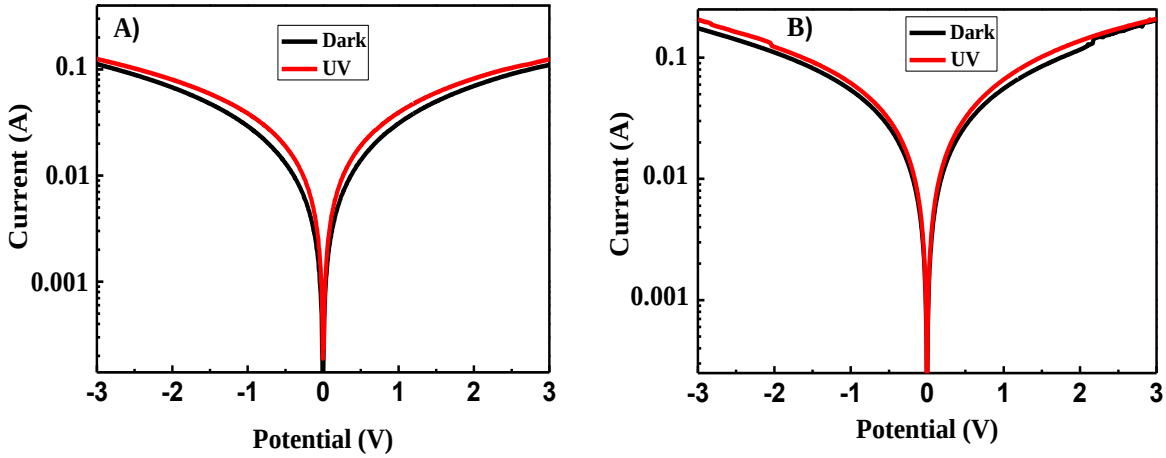


Figure 6. I-V curves of: (A) ZnO NWs and (B) U-ZnO NWs under dark (black curves) and UV illumination (red curves).

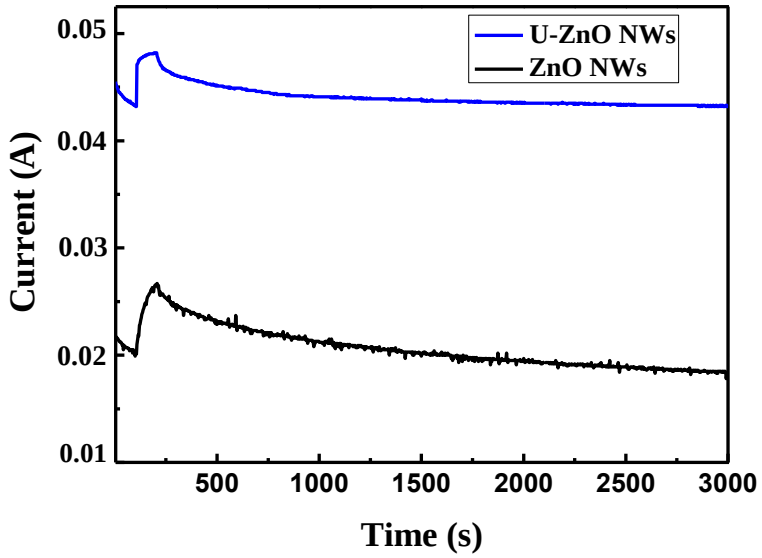


Figure 7. Intensity versus time curves under UV illumination at 365 nm for ZnO NWs and U-ZnO NWs materials

Table 1. Values of I_{Dark}, I_{UV} with I_{Dark}/I_{UV} current ratio at -1 V bias, UV photo-response current and UV photo-response for ZnO NWs and U-ZnO NWs.

Samples	I_{Dark}(A)	I_{UV}(A)	I_{UV}/I_{Dark}	ΔI(A)	UVphoto-response (A/W)
ZnO NWs	0.020 ± 10^{-4}	0.026 ± 5.10^{-4}	1.280 ± 0.03	0.026 ± 0.001	20.51 ± 0.25
U-ZnO NWs	0.037 ± 10^{-5}	0.042 ± 10^{-5}	1.110 ± 0.002	0.048 ± 0.002	36.81 ± 0.16